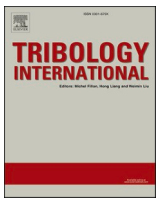
Tribology International 180 (2023) 108231



Contents lists available at ScienceDirect

Tribology International

journal homepage: www.elsevier.com/locate/triboint





Investigation of microstructure, wear and transverse rupture strength of WE43/nano B_4C composites produced by powder metallurgy method

Ufuk Tasci [a,b,*], Taha Alper Yilmaz [a], Bulent Bostan [c]

[a] Department of Technical Sciences Vocational School, Gazi University, 06374 Ankara, Turkey
[b] Department of Graduate School of Natural and Applied Sciences, Gazi University, 06500 Ankara, Turkey
[c] Department of Metallurgy and Materials Eng., Gazi University, 06500 Ankara, Turkey

ARTICLE INFO

Keywords:
WE43 alloy
B_4C
Mechanical properties
Wear

ABSTRACT

In this study, nano B_4C powder metal composite samples reinforced in WE43 matrix with different ratios (0.25, 0.5, 1 and 2 wt%) were produced by hot pressing method. The composite powders were mixed at 300 rpm for 4 h and produced by pressing under 350 MPa pressure in a hot pressing unit at 525 °C for 90 min. XRD, optical microscope and SEM-EDS devices were used for the characterization processes of nano B_4C reinforced composite samples. Microhardness, transverse rupture strength and wear were applied to determine the mechanical properties. It was determined that the highest hardness, transverse rupture strength and lowest wear rate were in WE43/2% nano B_4C composite sample.

1. Introduction

Magnesium (Mg) and its alloys have properties such as low density, high strength-to-weight ratio, high thermal conductivity, vibration damping capacity and recyclability [1,2]. Due to the lightness of Mg and its alloys, it is widely used in the aerospace, automotive and aerospace industries [3–5]. Despite such properties, Mg and its alloys are weak properties, such as less wear resistance, poor corrosion resistance, less strength at high temperatures, low ductility and minimum modulus of elasticity. In order to improve the aforementioned weak properties, alloys formed by adding rare earth elements into Mg have started to be developed in recent years [6–9]. Among the alloys developed with rare earth elements, WE43 and WE54 alloys, which are Mg-Y-RE (rare earth metals) systems, stand out [10–12]. WE43 contains other rare elements such as Neodymium (2.4–4.4 wt%), yttrium (3.7–4.3 wt%), zirconium (>0.4 wt%), and trace amounts of gadolinium [6,7,12]. WE43 alloy is used in stents, bone implants, and biodegradable screws in healthcare applications. It is also preferred in fields such as sport cars, aircraft engines and gearboxes, and helicopter transmissions [13,14]. Although neodymium, yttrium and other rare earth elements exhibit properties such as good mechanical performance at high temperatures, flame retardancy and high temperature creep resistance, studies are continuing to improve the problems in wear properties [15]. It increases the wear resistance and strength by adding ceramic reinforcements, such as the most commonly used (B_4C, SiC, TiC, Al_2O_3 etc.) to the Mg matrix [10,16–18]. Nano boron carbide (nB_4C) among ceramic particles is used in transport vehicles, light armor applications and nozzles with its high hardness, low density and high modulus of elasticity [11,19]. nB_4C is very hard, strong, resistant to chemicals and has a low density (2.51 g/cm^3) [8,20]. nB_4C, which is used as a reinforcement in the Mg matrix, increases the wear resistance [20,21]. There are several production methods for Mg-MMCs. These are infiltration, powder metallurgy and stirred casting methods [22]. Problems can be experienced in the process of homogeneously dispersing the ceramic particles in the metal matrix with mixing casting and infiltration methods. However, such problems can be easily overcome by using ball mills in the Powder Metallurgy (PM) method, and at the same time, the wettability can be improved by homogeneously dispersed [23–28]. Ceramic-reinforced metal matrix composites (MMCs) can show very good mechanical and wear properties when compared to non-reinforced metals [29,30]. MMCs with ceramic reinforced Mg matrix have better specific strength and minimum weight [31].

Behnian et al. in their study, they produced multi-walled carbon nanotubes and B_4C reinforced MMC. The situation they mentioned in the conclusion part of the study is that there is an improvement in both hardness and wear behavior depending on the increased B_4C ratio [18]. Sun et al. In their study, they produced nano graphene and B_4C hybrid ceramic reinforced MMC into Mg matrix by using PM method. The

* Corresponding author at: Department of Technical Sciences Vocational School, Gazi University, 06374 Ankara, Turkey.
E-mail address: ufuktasci@gazi.edu.tr (U. Tasci).

https://doi.org/10.1016/j.triboint.2023.108231
Received 14 November 2022; Received in revised form 14 December 2022; Accepted 6 January 2023
Available online 9 January 2023
0301-679X/© 2023 Elsevier Ltd. All rights reserved.

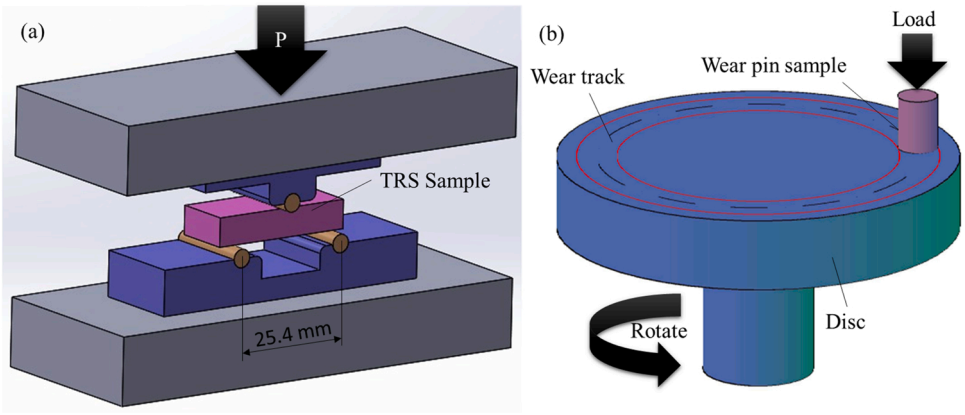


Fig. 1. (a) TRS test and (b) wear test setup on composite materials produced in the study.

authors stated that the hardness of the structure increased depending on the increasing B_4C ratio [16]. Ojalvo et al. In their study, they reported that nano B_4C reinforced MMC had higher wear resistance than non-reinforced materials [32]. According to Karakoc et al. They produced B_4C particle reinforced composite materials by PM method and stated that the wear rate decreased due to increasing B_4C reinforcement rates [33]. For the WE43 alloy, Benijamali et al. In their study, they produced B_4C reinforced composite samples using the stir casting method into WE43 matrix. When they examined the wear properties of the samples produced in their study, they stated that with the increase in the reinforcement ratio, the friction coefficient decreased and the wear resistance improved significantly. They also reported that abrasive and oxidation affect the wear properties of the matrix alloy when low load is used [34].

It is well known that the fabrication of composites reinforced with various ceramic particles (B_4C, SiC, Al_2O_3, etc.) in Mg alloys is carried out by stir casting and PM methods [3,34,35]. Wang et al. reported in their studies that homogeneous distribution of ceramic particles reinforced in Mg matrix is a general problem [36]. To overcome such problems, high-energy ball mixers are used in the PM method. Proper distribution of ceramic particle reinforcement with the used mixers improves the mechanical properties and wear performance. In addition, no research results were found in the literature on the fabrication of nanosized ceramic particle reinforced composite with 3D high energy ball mixers using PM method.

Thus, it is possible to produce the PM method with the desired size and the low cost compared to the casting method. In this study, transverse rupture strength (TRS) and wear properties were improved by adding homogeneously dispersed nB_4C into the WE43 alloy, which has a light, high temperature creep resistance and flame retardancy properties. It is aimed to increase the use of WE43/nB_4C composites produced by the hot pressing method in industrial applications.

2. Experimental procedure

2.1. Production method of composite specimens

The WE43 powder (Mg-4Y-3RE-Zr) with an average diameter of 45 μm was supplied by Magnesium Elektron™ ltd. The n B_4C (55 nm) was provided by Nanografi Nanotechnology™ and used for 0.25%, 0.5%, 1% and 2% n B_4C to prepare the composite powders. To mix the starting powders homogeneously, the mixing process was carried out for 4 h at a rotational speed of 300 rpm in a 3D ball mill with an atmospherically controlled chamber with a powder to ball ratio of 1/5. Y-coated Zr_2O_3

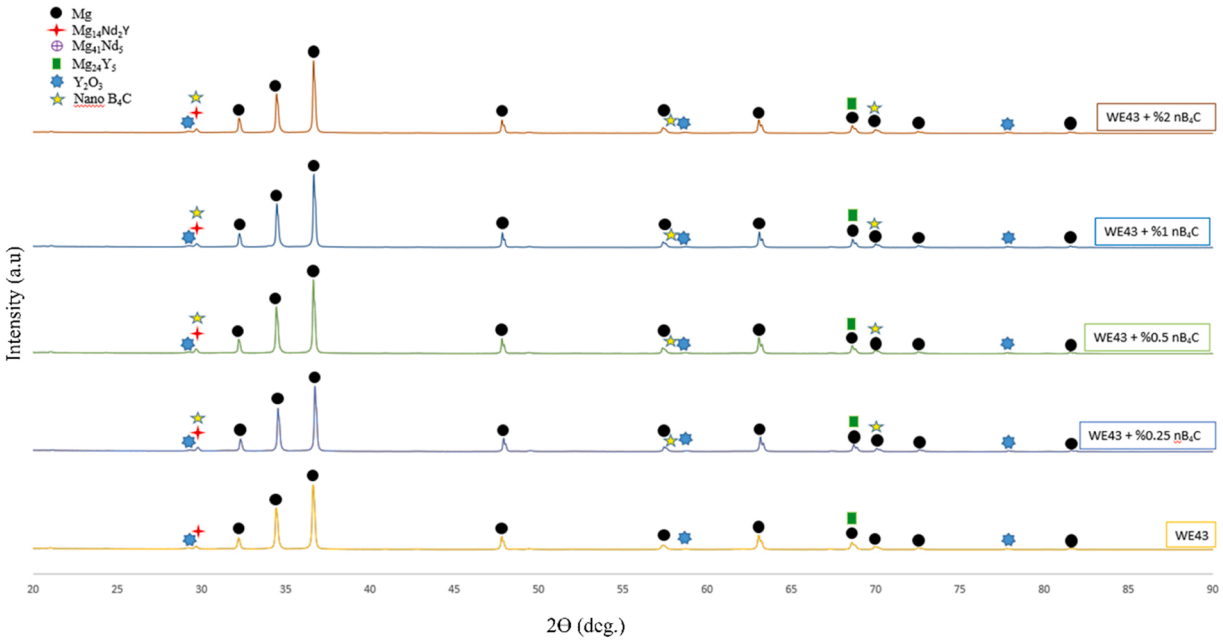


Fig. 2. XRD patterns of WE43 alloy and WE43/nB_4C composites.

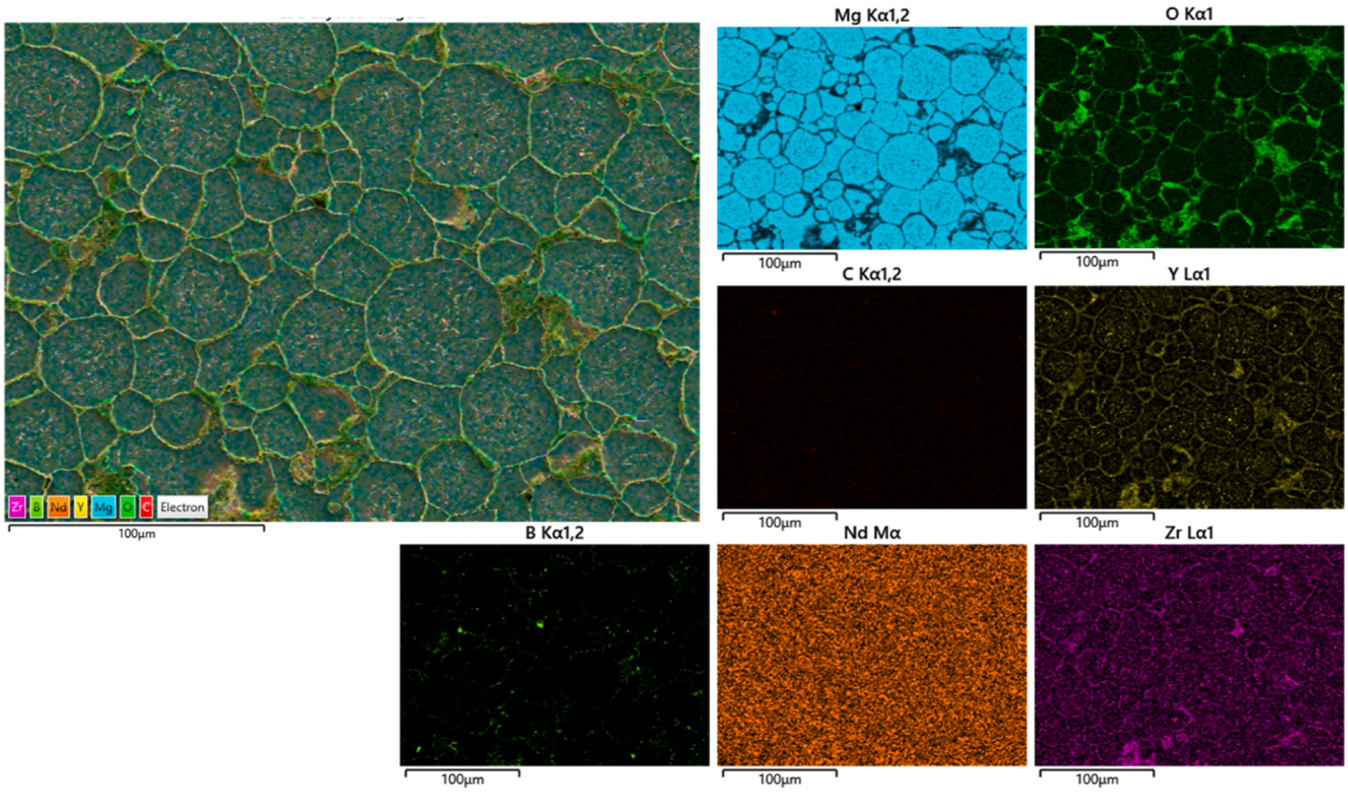


Fig. 3. Mapping analysis result of WE43/2% nB_4C composite material.

spheres were used for the mixing process. The powders with different ratios of nB_4C in the WE43 alloy were prepared by hot pressing. A custom-made graphite mold was used to press the powders. The powders placed in the mold were first precompressed at a pressure of 10 MPa at room temperature. The mixed composite powders were then pressed under a load of 350 MPa at 525 °C for 90 min. The heating rate was set at 10 °C per minute. After hot pressing, specimens with a size of 40x40x10 mm^3 were produced.

2.2. Microstructure and mechanical analysis

The powder metal block specimens prepared after hot pressing were cut by electrical discharge machine (EDM) to prepare specimens for microstructure investigation, hardness, TRS and abrasion tests. A series of preliminary work was carried out to investigate the microstructure of the composites. First, grinding was performed with SiC papers, followed by polishing with anhydrous solutions. Final polishing was done with an alkaline suspension of fumed silica (0.2 μm). Etching was performed in 0.7 mL H_3PO_4 + 4 g picric acid + 100 mL ethanol (95%) according to ASTM-E407/121 standards for 5 s. FE-SEM and EDS analyzes of the metallographically prepared samples were performed using a scanning electron microscope model ZEISS GeminiSEM 500. For phase analysis, X-ray diffraction analyzes were performed using a Bruker D8 Advance X-ray diffractometer (XRD). After the microstructural analyzes of the samples, the hardness measurements were performed according to ASTM E-384 [37]. A total of 10 hardness measurements (HV0.5) were made on the surface of the composites at 3 mm intervals to calculate the average values. For the TRS test, 3 specimens of each composite material with dimensions 6.45 × 12.7 × 31.2 mm^3 were prepared according to the MPFI-41, 1998 standard [38]. Instron MFL brand universal testing machine with a capacity of 200 kN was used for testing TRS at room temperature and strain rate of 1 mm/min. In the wear tests, for each parameter, 3 specimens with a diameter of 10 mm and a height of 10 mm were abraded in the tribometer T10/20 abrasion tester according to the ASTM G99–05 standard [39]. The wear tests were performed on a Hardox 400 steel plate over a distance of 1000 m under a load of 15 N. In wear tests, weight loss values were measured using an electronic balance with a sensitivity of 0.0001 mg. Fig. 1. show the schematic diagram of TRS test and wear test.

3. Results and discussion

3.1. Microstructural analysis

The XRD patterns of the WE43 alloy and the WE43/nB_4C composites prepared by hot pressing are shown in Fig. 2. Examination of the XRD peaks shows that the fabricated composites contain $Mg_{24}Y_5$ and $Mg_{41}Nd_5$ intermetallic phases and an α-Mg matrix phase. The matrix alloy in the XRD samples was found to increase slightly with the addition of nB_4C particles and to have additional peaks corresponding to nB_4C. In addition, phases such as magnesium oxide and magnesium diboride were not detected, which is considered as evidence of the effectiveness of the method used [40–43].

When the FE-SEM /MAP microstructure of the WE43 alloy was examined, it was found that intermetallic phases had formed at the grain boundaries and in the grain interior (Fig. 3). It was found that especially the precipitates at the grain boundaries are rich in Nd and Y, which are fixed and homogeneously distributed in the matrix structure of the nB_4C ceramic particles.

SEM microstructure images of WE43 alloy and WE43/nB_4C composites were examined in Fig. 4, showing that the α-Mg matrix was surrounded by a eutectic second phase and consisted of small precipitates randomly distributed in the alloy. Patchy areas such as localized white dendrites were observed in the grains [44]. During sintering, Y_2O_3 was found to be formed in the form of on the surface and grain boundaries from Y in the solid solution [40,45]. They form a continuous network along the grain boundaries, which may be due to Y migrating to previous particle surfaces attracted by oxygen [46,47]. Depending on

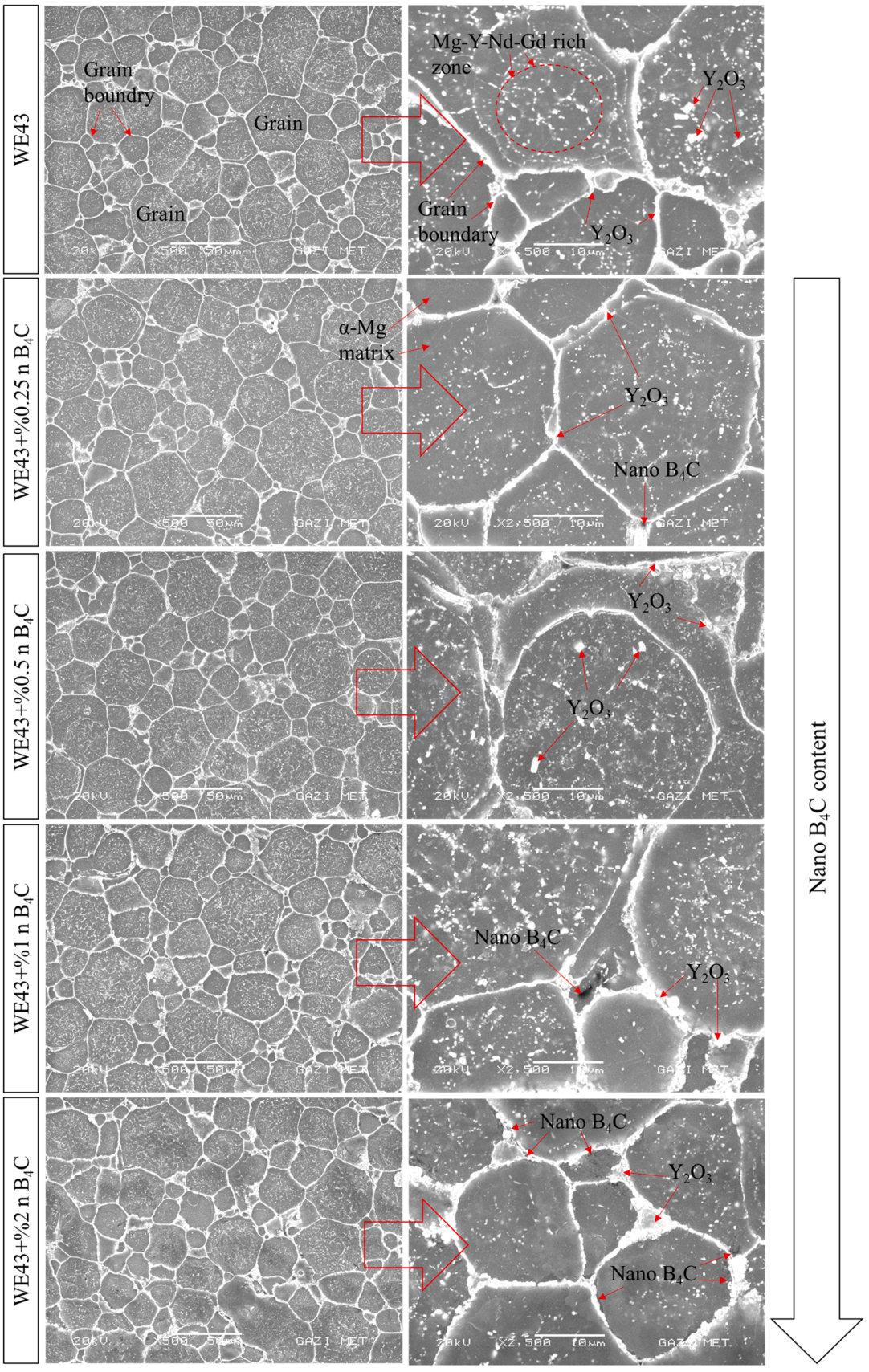


Fig. 4. SEM microstructure images of WE43 alloy and WE43/nB_4C composite materials.

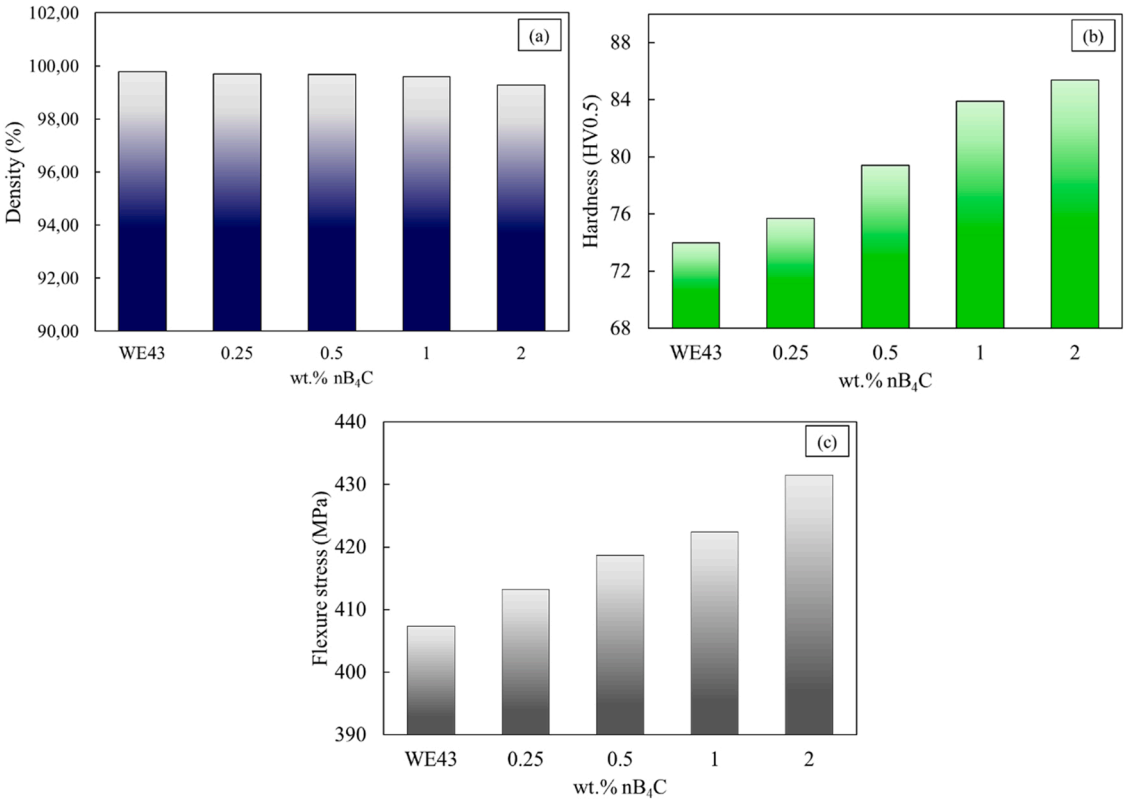


Fig. 5. Density (a), hardness (b), and TRS (c) of the composite materials.

the diffusion distance and temperature effect, this situation is more common in small grains. Moreover, it was observed that the density of eutectic phases at grain boundaries increased with increasing nB_4C ratio at grain boundaries. Although the powder grains used are spherical, their shape is no longer spherical during hot pressing, but has changed to a polygonal shape during sintering.

3.2. Physical and mechanical properties

When examining the density curve (Fig. 5a) of WE43 alloy and WE43/nB_4C composites, it was found that the lowest density was present in WE43 alloy (99.00%) and the highest density was present in WE43/2% nB_4C composite (99.49%). It was found that the densities of the nanoceramic particle reinforced composites increased compared to the unreinforced materials. The reason for this is probably the higher density of the B_4C ceramic particles compared to the WE43 matrix alloy [48]. From the graph, it can be seen that the density increases with increasing amount of nB_4C additions. It is assumed that the formation of an effective bond between the ceramic particles and the matrix, the good wettability of the particles with the matrix, and the distribution of reinforcement lead to a decrease in porosity. When the hardness results (Fig. 5b) were examined, it was found that the unreinforced WE43 alloy had a hardness of 74 HV, while the hardness of sample reinforced with WE43/2% nB_4C increased by about 16% and reached to 85.7 HV.

By examining the results of TRS (Fig. 5c), it was found that the bending stress values increase with increasing reinforcement ratio in the same way as the density and hardness values [49]. Compared to the 407.4 MPa strength of the WE43 alloy, the WE43/2% nB_4C sample exhibited the highest strength of 431.5 MPa, an increase of about 6%. With the increase in hardness values, it was observed that the results of

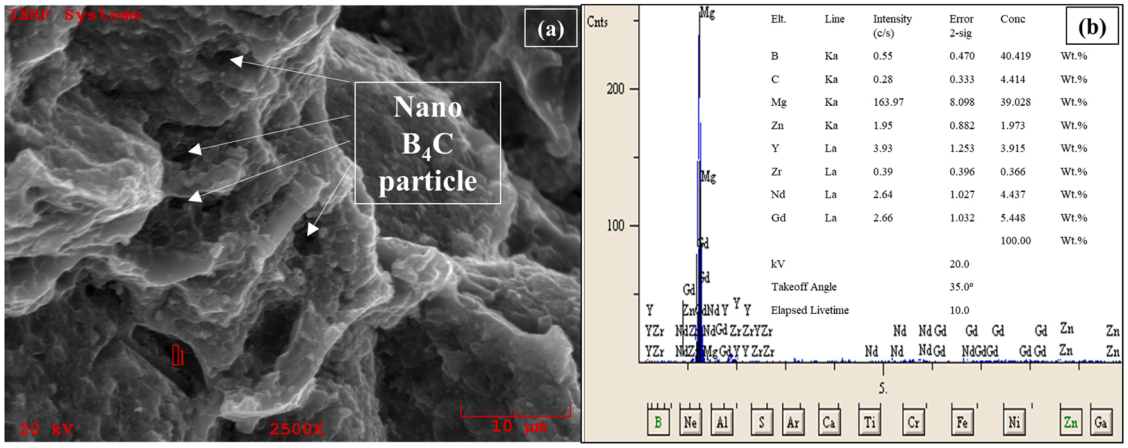


Fig. 6. (a) SEM image of the fracture surface of WE43/2% nB_4C composite materials after TRS test, (b) EDS analysis result.

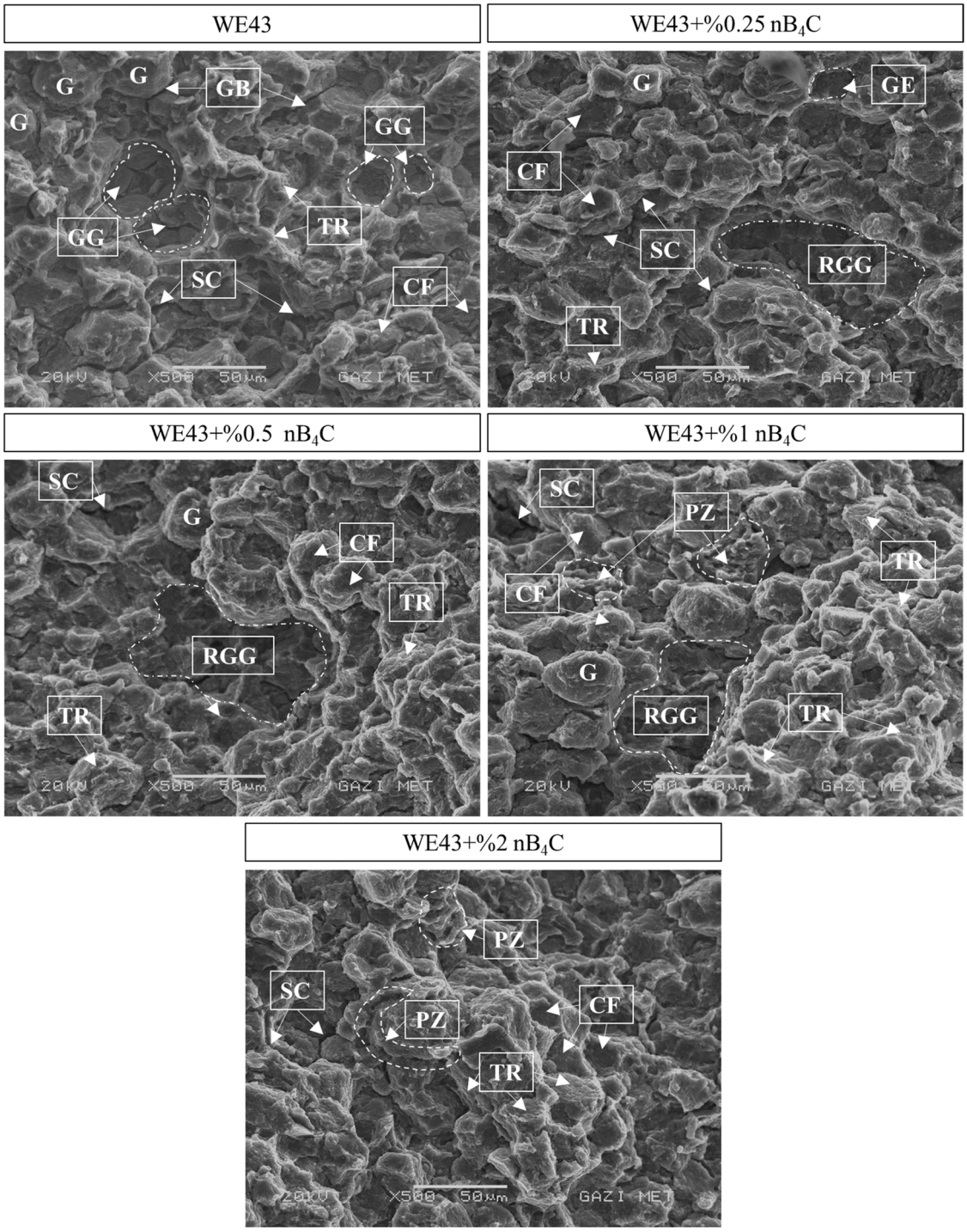


Fig. 7. SEM images of the fracture surface of WE43 alloy and WE43/nB_4C composite materials after TRS test.

TRS also increased and strengthened the material. It can be said that one of the reasons for this increase is that the hard B_4C particles prevent the movement of grain boundaries during deformation and restrict the plastic flow of the matrix. As the amount of particles increases, this effect is exacerbated by the reduction in interparticle spacing. Another factor affecting the increase in TRS values is the increase in dislocation density due to the increase in particle fraction. The dislocation interaction resulting from the increased dislocation density leads to strain hardening of the matrix. In composites with added ceramic particles, the homogeneous distribution of ceramic particles increases the strength by preventing dislocation movement through the Orowan mechanism. At the same time, it is known that the mechanical properties improve with increasing amounts of reinforcement in these materials [50,51]. In this study, the ceramic particles were homogeneously distributed in the microstructure by ball milling and increased the TRS, by preventing the dislocation movement. nB_4C, as the hardest material after diamond, led to the improvement of the mechanical properties of ductile WE43 with its homogeneous distribution.

3.3. *Fractured surface analysis*

Fig. 6 shows the SEM images and the EDS result taken from the

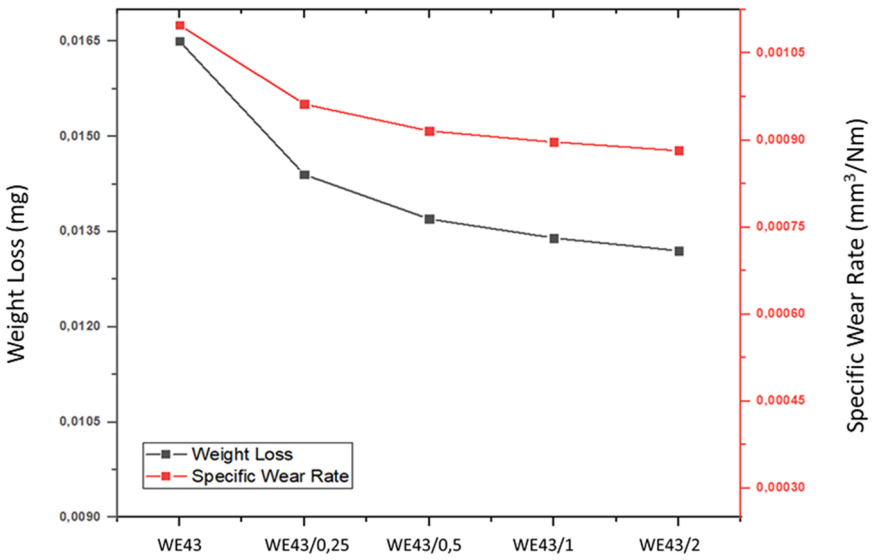


Fig. 8. Graph of (a) volume loss (b) specific wear rate of WE43 alloy and WE43/nB_4C composite materials.

fracture surface of the composite WE43/2% nB_4C. According to the EDS result of point 1, the intense boron peak indicates the presence of nB_4C particles. From the image of the fracture surface, it can be seen that the nB_4C particles are distributed on the grain surface.

In Fig. 7, SEM images of the fractured surfaces of all e TRS test samples are shown. By examining of the images of the fracture surface of the WE43 alloy without ceramic reinforcement, it is clear that the fracture occurs at the grain boundaries. It is known that the Y_2O_3 phase in the microstructure of the WE43 alloy presents at the grain boundaries. Since this phase is harder and more brittle than the base material, it is assumed that the cracking and fracture occurs at the grain boundaries during the TRS test [52]. Secondary cracks can be seen on the fracture surface of WE43 alloy. The grain gaps formed on the fracture surface show that the grains correspond to the other fracture surface (grain gap). In materials that break from the grain boundary, the grains can be seen on the two fracture surfaces [53]. In addition, grain gap formations have been observed in some areas of composite materials. In WE43 materials with the addition of ceramic particles nB_4C, the fractures are partly within the grain boundaries and partly within the grain. The main reason for this is that the nB_4C particles increase the strength of the grain boundaries by dispersion strengthening at the grain boundaries [54]. While the fracture surfaces of the WE43 alloy have a clean grain boundary, the fracture surfaces of the nB_4C-reinforced composites become increasingly rough. The nB_4C particles carry the applied load during the TRS test because they are located at the grain boundaries. As the ratio of ceramic particles and nB_4C reinforcement increases, especially for WE43/nB_4C composites with 1% and 2% nB_4C reinforcement, a particle zone is formed. When examining the composite with 2% nB_4C, it can be seen that the nB_4C particles are arranged around the fracture grain. In Fig. 7, crack edge formations can be seen in some areas and cleavage catastrophe formations in other areas. Due to the increase in nB_4C ratio, cleavage excrement formations can be seen on the fracture surface. Cleavage phenomena are caused by hard phases at grain boundaries, which are particularly brittle [55]. Intragranular fractures are observed to form crack edges.

3.4. Tribological behavior

3.4.1. Wear rate

Fig. 8 shows the weight loss and specific wear rates of the unreinforced WE43 matrix alloy and the WE43/nB_4C composites with different reinforcements under 15 N load. The weight loss and specific wear rates decrease with increasing reinforcement ratio relative to the matrix material. In addition, the applied wear tests show that the composites have lower wear rates than the matrix alloy. Moreover, a decrease in wear rates was observed when the nB_4C reinforcement ratio increased from 0.25 to 2 wt%. It is well known that various properties such as grain size, porosity in microstructure, strength and hardness affect the wear behavior of materials. While the specific wear rates for the unreinforced WE43 alloy is $1.09 * 10^{-6}$ mm^3/Nm, for the WE43/2% nB_4C composite alloy, it is $8.81 * 10^{-7}$ mm^3/Nm. It is assumed that the reinforcement particles act as a coercive factor at the grain boundaries, leading to the development of wear resistance [50].

3.4.2. Wear mechanisms

SEM / EDS analysis was performed to investigate the mechanisms of WE43 alloy and WE43/nB_4C composites during wear testing and the effects of the presence of nB_4C particles in different proportions on wear behavior. The 3D profilometer scan was performed on the worn surfaces to determine the sample with the best wear behavior among the matrix alloy and composite samples. Fig. 9 shows the friction coefficient-wear distance changes of MMCs reinforced with nB_4C into WE43 matrix at different rates and without reinforcement. The parameters were kept constant to determine the effects of B_4C particle reinforcement on the wear resistance of MMCs. It is seen that the friction coefficient values decrease with the increase in the reinforcement ratio in the composites. In addition, it was determined that the highest friction coefficient value was in the unreinforced WE43 alloy. The increase in the hardness values along with the increase in the amount of nB_4C in the matrix and the decrease in the friction coefficient values show parallelism [56]. According to the Archard equation, it is expected that the wear rate and friction coefficient decrease in composites with increasing hardness [57].

The SEM and surface profile images of the worn surfaces of the WE43 alloy and WE43/nB_4C composite subjected to the wear test under a load of 15 N are shown in Fig. 10. Upon examination of the images, a series of grooves parallel to the sliding direction, debris, plastic deformation, and significant crater areas were visible on the worn surface of the unreinforced WE43 matrix alloy. This situation is considered to exhibit typical abrasive wear characteristics. In addition, wear was found to be more severe in the oxidized areas. It is believed that the Y and Gd elements in the WE43 alloy, which has a low oxidation activation energy, along with the frictional heat that occurs during wear, cause the formation of oxidized areas. It is believed that the non-ceramic reinforced WE43 alloy material undergoes more deformation than other ceramic-reinforced specimens after the wear test [3]. Examining Fig. 10. due to the

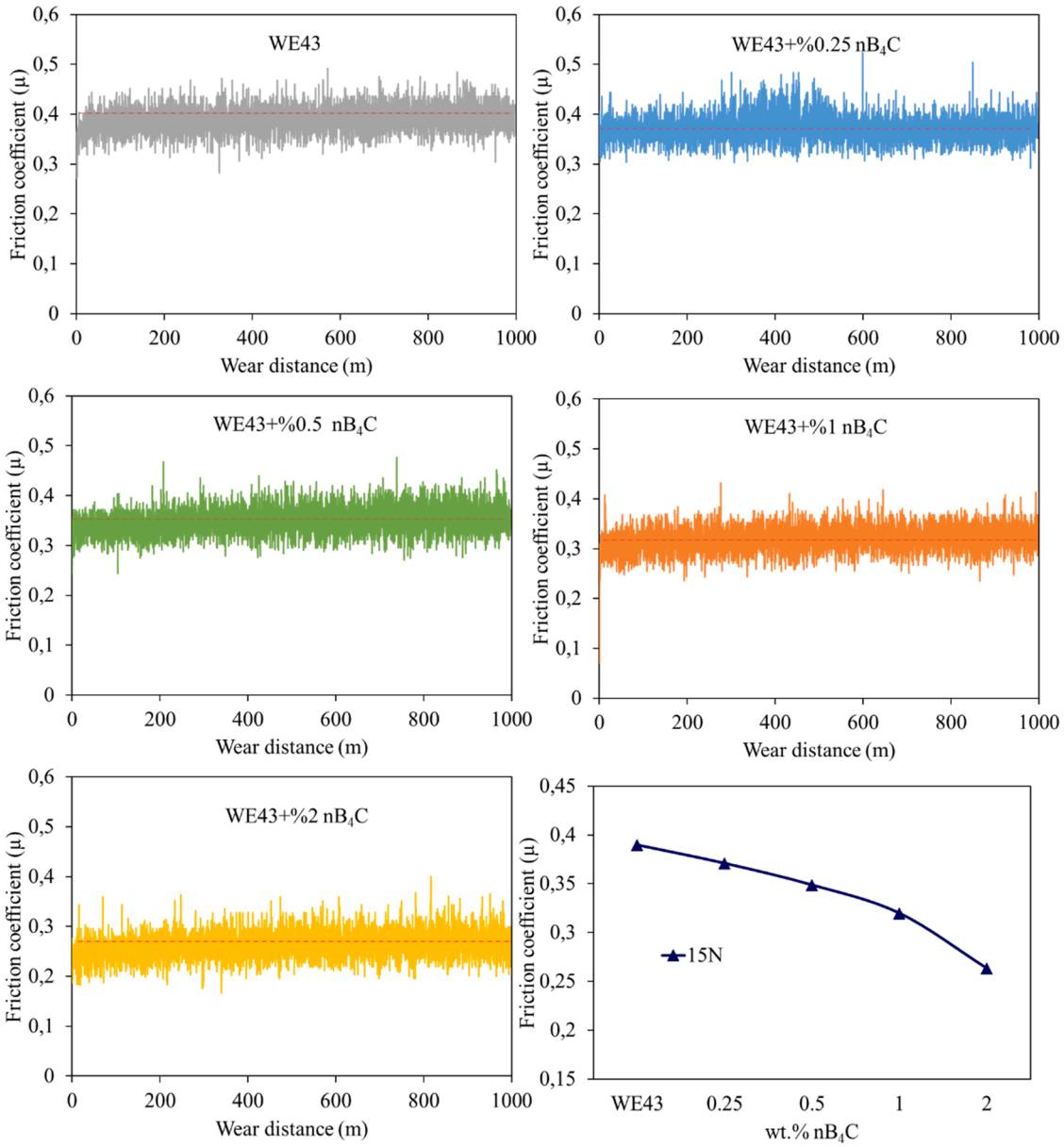


Fig. 9. Graph of coefficients of friction of WE43 alloy and WE43/nB_4C composite materials.

increasing ceramic reinforcement ratio, it can be seen that the composite specimen WE43/2% nB_4C has the lowest friction coefficient and volume loss compared to the other specimens, as indicated in Fig. 9. The reason is that both the oxide layer formed in the structure during wear and the nB_4C in the matrix play a challenging role during wear. It is believed that the deep grooves increase mainly with increasing levels of reinforcement, but show better wear behavior compared to the other specimens. In addition to the fact that nB_4C.

is responsible for the formation of grooves, intermetallic phases such as yttrium oxide (Y_2O_3) that form at the grain boundaries are believed to play a role in these groove formations [34].

The results of the 3D profilometer analysis and the surface roughness values of the WE43 matrix and the WE43/nB_4C composite specimens are shown in Fig. 11. When the Ra values of all samples were examined, they were found to be compatible with the results of friction coefficient (FC), weight loss (VL) and specific wear rate (SWR) as the reinforcment ratio increased. As can be seen from the 3D isometric images, deep grooves increased and affected the Ra value in the sample with 2% nB_4C, and the decrease of color distribution in the isometric surface image of the wear samples also supports the Ra values along with the increasing reinforcement ratios of surface roughness.

4. Conclusion

The study of the microstructure, wear behaviour and transversre Rupturre strength of WE43 and WE43/nano B_4C composites produced by the powder metallurgical process leads to the following conclusions:

1. While the highest density value is observed in the unreinforced WE43 alloy (99.00%), the density values decrease with increasing nB_4C particle addition. The lowest density value was observed in WE43/2% nB_4C composite (97.49%).

2. When the microstructure was examined, it was found that the eutectic phases at the grain boundaries formed more strongly with increasing nB_4C content.

3. The mixing prosess in atmospherically controlled 3D ball mill it was seen in the microstructure showed that the nB_4C particles were homogeneously distributed at the grain boundaries.

4. While the lowest hardness occurred in the unreinforced WE43

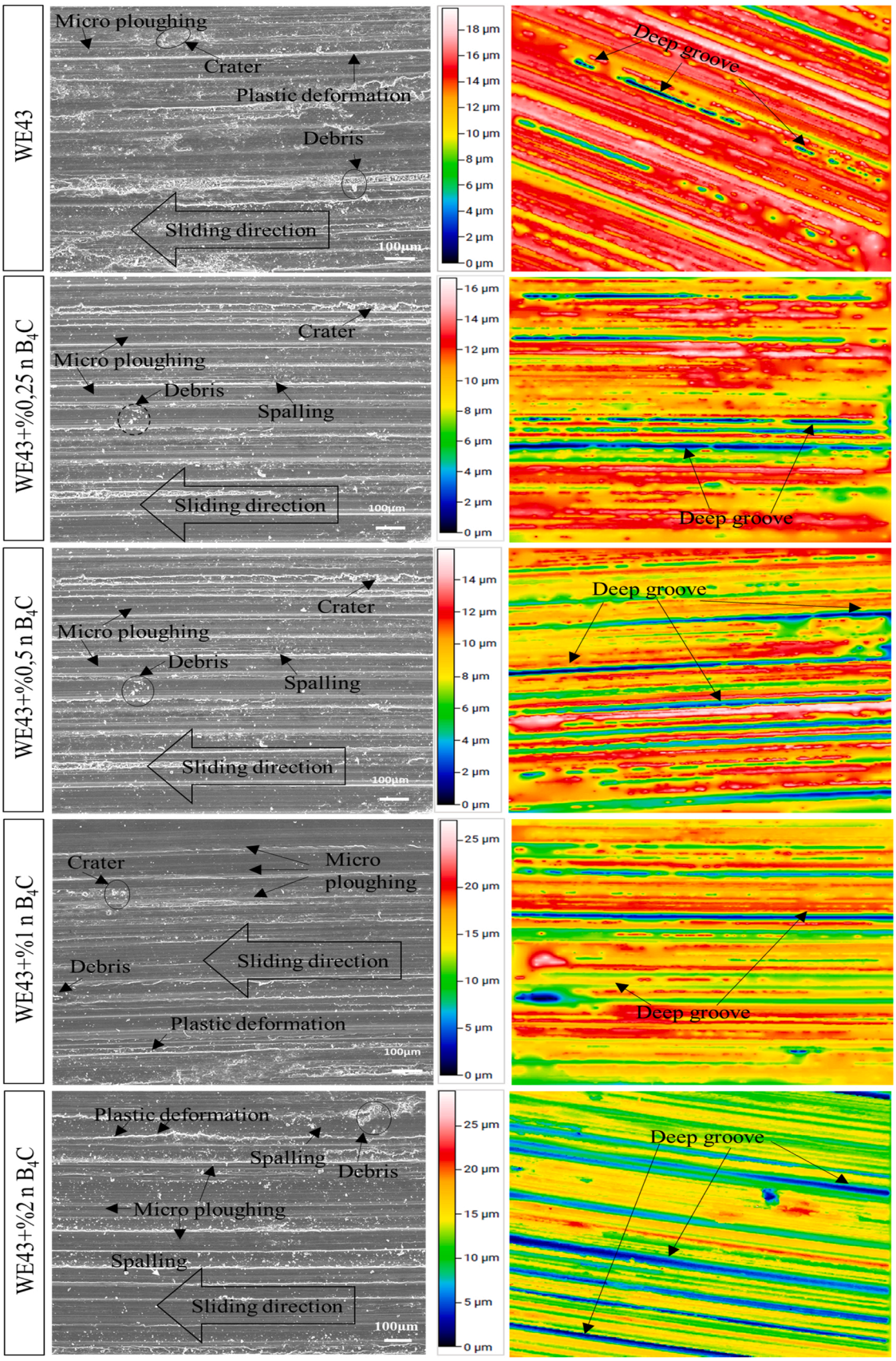


Fig. 10. Worn surface SEM pictures and 3D isometric images of the wear tracks.

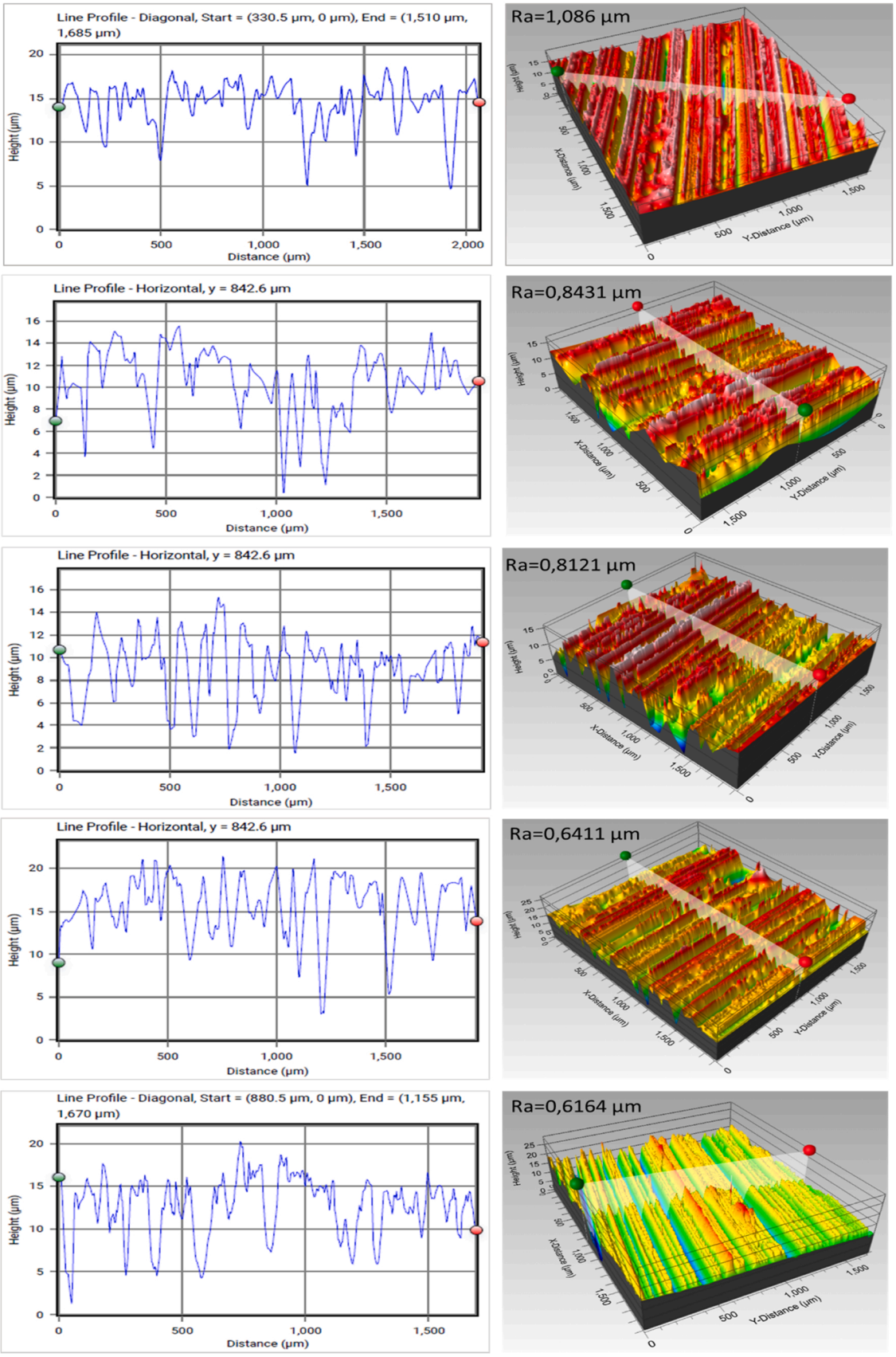


Fig. 11. Surface roughness (Ra) and 3D isometric images of worn surfaces of WE43 alloy and WE43/ nB_4C composite.

alloy, the highest hardness was observed in the WE43/ 2% nB$_4$C composite. It was observed that the hardness values increased with increasing nB$_4$C ratio.

5. It was found that the transverse rupture strength improved with increasing nB$_4$C ratio. The homogeneous distribution of nB$_4$C particles at the grain boundaries increased the strength of the grain boundaries.

6. The addition of nB$_4$C particles improved the wear resistance and minimized the volume losses. While the lowest specific wear rate was seen in 2% nB$_4$C composite, the highest specific wear rate occurred with the WE43 alloy.

Declaration of Competing Interest

The authors declare that they have no known competing financial interests or personal relationships that could have appeared to influence the work reported in this paper.

Data Availability

Data will be made available on request.

Acknowledgments

This study has been financially supported by the Gazi University Scientific Research Projects Coordination Unit [under Project Number FDK-2021–7400].

References

[1] Qian M, Hildebrand ZCG, StJohn DH. The loss of dissolved zirconium in zirconium-refined magnesium alloys after remelting. Metall Mater Trans A 2009;40:2470–9.
[2] Chen Q, Zhao Z, Shu D, Zhao Z. Microstructure and mechanical properties of AZ91D magnesium alloy prepared by compound extrusion. Mater Sci Eng: A 2011; 528:3930–4.
[3] Xie Z, Guo F, Huang X, Li K, Chen Q, Chen Y, et al. Understanding the anti-wear mechanism of SiCp/WE43 magnesium matrix composite. Vacuum 2020;172: 109049.
[4] Zheng T, Hu Y, Pan F, Zhang Y, Tang A. Fabrication of corrosion-resistant superhydrophobic coating on magnesium alloy by one-step electrodeposition method. J Magnes Alloy 2019;7:193–202.
[5] NasiriVatan H, Ebrahimi-Kahrizsangi R, Asgarani MK. Tribological performance of PEO-WC nanocomposite coating on Mg alloys deposited by plasma electrolytic oxidation. Tribol Int 2016;98:253–60.
[6] Senocak TC, Yilmaz TA, Budak HF, Gulten G, Yilmaz AM, Ezirmik KV, et al. Influence of sodium pentaborate ($B_5H_{10}NaO_{13}$) additive in plasma electrolytic oxidation process on WE43 magnesium alloys, Materials Today. Communications 2022;30:103157.
[7] Hamdy Makhlouf AS. Intelligent Stannate-Based Coatings of Self-Healing Functionality for Magnesium Alloys. In: Tiwari A, Rawlins J, Hihara LH, editors. Intelligent Coatings for Corrosion Control. Butterworth-Heinemann, Boston; 2015. p. 537–55.
[8] Arslan G, Kara F, Turan S. Quantitative X-ray diffraction analysis of reactive infiltrated boron carbide–aluminium composites. J Eur Ceram Soc 2003;23: 1243–55.
[9] Yao YT, Chen LQ. Processing of B$_4$C particulate-reinforced magnesium-matrix composites by metal-assisted melt infiltration technique. J Mater Sci Technol 2014; 30:661–5.
[10] Krishnan MN, Suresh S, Vettivel SC, Prema CE, Jesuthanam CP, Novel A. Image processing technique for analyzing wear worn surface roughness and corrosion behavior of sintered Mg/B$_4$C composites. T Indian I Met 2021;74:51–68.
[11] Cafri M, Dilman H, Dariel MP, Frage N. Boron carbide/magnesium composites: Processing, microstructure and properties. J Eur Ceram Soc 2012;32:3477–83.
[12] Soderlind J, Cihova M, Schaublin R, Risbud S, Loffler JF. Towards refining microstructures of biodegradable magnesium alloy WE43 by spark plasma sintering. Acta Biomater 2019;98:67–80.
[13] Castellani C, Lindtner RA, Hausbrandt P, Tschegg E, Stanzl-Tschegg SE, Zanoni G, et al. Bone–implant interface strength and osseointegration: biodegradable magnesium alloy versus standard titanium control. Acta Biomater 2011;7:432–40.
[14] Kubasek J, Dvorsky D, Cavojsky M, Roudnicka M, Vojtech D. WE43 magnesium alloy - material for challenging applications. Kov Mater 2019;57:159–65.
[15] Dvorsky D, Kubasek J, Vojtech D, Cavojsky M. Advanced mechanical and corrosion properties of WE43 alloy prepared by powder metallurgy. Acta Phys Pol A 2018; 134:748–52.
[16] Sun Y, Cevik E, Turen Y, Ahlatci H, Turan ME, Aydin F, et al. Influence of GNPs and B$_4$C reinforcements on mechanical, thermal and wear properties of magnesium matrix composite produced by powder metallurgy. J Compos Mater 2021;55: 3881–91.
[17] Sankar C, Gangatharan K, Singh SCE, Sharma RK, Mayandi K. Optimization on tribological behaviour of milled nano-B4C particles reinforced with AZ91 alloy through powder metallurgy method. T Indian I Met 2019;72:1255–75.
[18] Behnamian Y, Serate D, Aghaie E, Zahiri R, Tolentino Z, Niazi H, et al. Tribological behavior of ZK60 magnesium matrix composite reinforced by hybrid MWCNTs/ B$_4$C prepared by stir casting method. Tribol Int 2022;165.
[19] Suresh S, Krishnan MN, Vettivel SC. Effect of B$_4$C on strength coefficient, cold deformation and work hardening exponent characteristics of Mg composites. J Magnes Alloy 2022;10:1381–400.
[20] Moheimani SK, Keshtgar A, Khademzadeh S, Tayebi M, Rajaee A, Saboori A. Tribological behaviour of AZ31 magnesium alloy reinforced by bimodal size B$_4$C after precipitation hardening. J Magnes Alloy 2021.
[21] Selvakumar N, Ramkumar T. Effects of high temperature wear behaviour of sintered Ti–6Al–4V reinforced with nano B$_4$C particle. T Indian I Met 2016;69: 1267–76.
[22] Aydin F, Sun Y, Ahlatci H, Turen Y. Investigation of microstructure, mechanical and wear behaviour of B$_4$C particulate reinforced magnesium matrix composites by powder metallurgy. T Indian I Met 2018;71:873–82.
[23] Zhou L, Xu F, Cai X, Chen Y, Guo L, Yue Y. Evolution of microstructure and mechanical properties of CNTs/Al-Mg composites prepared by powder metallurgy. Integr Ferroelectr 2022;228:1–8.
[24] Esquivel J, Wachowiak MG, O'Brien SP, Gupta RK. Thermal stability of nanocrystalline Al-5at%Ni and Al-5at%V alloys produced by high-energy ball milling. J Alloy Compd 2018;744:651–7.
[25] Alekhya C, Prajoshna A, Ayaz Baig M, Chandrika C, Devaraju A, Gadakary S. Preparation and characterization of Al-TiO2-Mg composites through powder metallurgy. Mater Today: Proc 2022;66:489–95.
[26] Farvizi M, Javan MK, Akbarpour MR, Kim HS. Fabrication of NiTi and NiTi-nano Al_2O_3 composites by powder metallurgy methods: comparison of hot isostatic pressing and spark plasma sintering techniques. Ceram Int 2018;44:15981–8.
[27] Seth PP, Singh N, Singh M, Prakash O, Kumar D. Formation of fine Mg2Si phase in Mg-Si alloy via solid-state sintering using high energy ball milling. J Alloy Compd 2020;821.
[28] Dvorsky D, Kubasek J, Roudnicka M, Prusa F, Necas D, Minarik P, et al. The effect of powder size on the mechanical and corrosion properties and the ignition temperature of WE43 alloy prepared by spark plasma sintering. J Magnes Alloy 2021;9:1349–62.
[29] Soltani HM, Tayebi M. Determination of wear parameters and mechanisms of diamond/copper tools in marble stones cutting. Int J Refract Met H 2020;87.
[30] Yadav M, Kumaraswamidhas LA, Singh SK. Investigation of solid particle erosion behavior of Al-Al_2O_3 and Al-ZrO2 metal matrix composites fabricated through powder metallurgy technique. Tribol Int 2022;172.
[31] Yao YT, Jiang L, Fu GF, Chen LQ. Wear behavior and mechanism of B$_4$C reinforced Mg-matrix composites fabricated by metal-assisted pressureless infiltration technique, T Nonferr Metal Soc 2015;25:2543–8.
[32] Ojalvo C, Zamora V, Moreno R, Guiberteau F, Ortiz AL. Transient liquid-phase assisted spark-plasma sintering and dry sliding wear of B$_4$C ceramics fabricated from B$_4$C nanopowders. J Eur Ceram Soc 2021;41:1869–77. https://doi.org/10.1520/E0010-15.
[33] Karakoc H, Ovali I, Dundar S, Citak R. Wear and mechanical properties of Al6061/ SiC/B$_4$C hybrid composites produced with powder metallurgy. J Mater Res Technol 2019;8:5348–61.
[34] Banijamali SM, Najafi S, Sheikhani A, Palizdar Y. Dry tribological behavior of hot-rolled WE43 magnesium matrix composites reinforced by B$_4$C particles. Wear, 508-2022;509:204487.
[35] Liu J, Suryanarayana C, Ghosh D, Subhash G, An L. Synthesis of Mg–Al2O3 nanocomposites by mechanical alloying. J Alloy Compd 2013;563:165–70.
[36] Wang X-j, Hu X-s, Nie K-b, Wu K, Zheng M-y. Hot extrusion of SiCp/AZ91 Mg matrix composites. T Nonferr Met Soc 2012;22:1912–7.
[37] Danish M, Gupta MK, Rubaiee S, Ahmed A, Korkmaz ME. Influence of hybrid Cryo-MQL lubri-cooling strategy on the machining and tribological characteristics of Inconel 718. Tribol Int 2021;163:107178.
[38] Karabulut Ş, Gökmen U, Çinici H. Study on the mechanical and drilling properties of AA7039 composites reinforced with Al_2O_3/B$_4$C/SiC particles. Compos Part B: Eng 2016;93:43–55.
[39] Naeem M, Diaz-Guillen JC, Khalid A, Guzman-Flores I, Munoz-Arroyo R, Iqbal J, et al. Improved wear resistance of AISI-1045 steel by hybrid treatment of plasma nitriding and post-oxidation. Tribol Int 2022;175.
[40] Tang B, Li J, Wang Y, Luo H, Ye J, Chen X, et al. Mechanical properties and microstructural characteristics of Ti/WE43 composites. Vacuum 2022;206:111534.
[41] Gangireddy S, Gwalani B, Liu K, Faierson EJ, Mishra RS. Microstructure and mechanical behavior of an additive manufactured (AM) WE43-Mg alloy. Addit Manuf 2019;26:53–64.
[42] Hyer H, Zhou L, Benson G, McWilliams B, Cho K, Sohn Y. Additive manufacturing of dense WE43 Mg alloy by laser powder bed fusion. Addit Manuf 2020;33.
[43] Manohar G, Pandey KM, Maity SR. Effect of microwave sintering on the microstructure and mechanical properties of AA7075/B$_4$C/ZrC hybrid nano composite fabricated by powder metallurgy techniques. Ceram Int 2021;47: 32610–8.
[44] Coy AE, Viejo F, Skeldon P, Thompson GE. Susceptibility of rare-earth-magnesium alloys to micro-galvanic corrosion. Corros Sci 2010;52:3896–906.
[45] Kubasek J, Dvorsky D, Cavojsky M, Vojtech D, Beronska N, Fousova M. Superior properties of Mg-4Y–3RE-Zr alloy prepared by powder metallurgy. J Mater Sci Technol 2017;33:652–60.
[46] Prikhna T, Eisterer M, Weber HW, Gawalek W, Chaud X, Sokolovsky V, et al. Pinning in $\hbox{MgB}_{2}$- and YBaCuO-based superconductors: effect of

manufacturing pressure and temperature. IEEE Trans Appl Supercond 2013;23. 8001605-8001605.
[47] Tong X, Wu GH, Zhang L, Wang YX, Liu WC, Ding WJ. Microstructure and mechanical properties of repair welds of low-pressure sand-cast Mg-Y-RE-Zr alloy by tungsten inert gas welding. J Magnes Alloy 2022;10:180–94.
[48] Venkatesan K, Ramanujam R, Joel J, Jeyapandiarajan P, Vignesh M, Tolia DJ, et al. Study of cutting force and surface roughness in machining of Al alloy hybrid composite and optimized using response surface methodology. Procedia Eng 2014; 97:677–86.
[49] Su W, Li S, Sun L. Effect of multilayer graphene as a reinforcement on mechanical properties of WC-6Co cemented carbide. Ceram Int 2020;46:15392–9.
[50] Ozer A. The microstructures and mechanical properties of Al-15Si-2.5Cu-0.5Mg/(wt%)B_4C composites produced through hot pressing technique and subjected to hot extrusion. Mater Chem Phys 2016;183:288–96.
[51] Wang D, Huang JH, Tan CL, Ma WY, Zou YM, Yang YQ. Mechanical and corrosion properties of additively manufactured SiC-reinforced stainless steel. Mat Sci Eng a-Struct 2022;841.
[52] Wang WL, Yang X, Wang KK. Research on formability, microstructure and mechanical properties of selective laser melted Mg-Y-Sm-Zn-Zr magnesium alloy. Mater Charact 2022;189.
[53] Kondori B, Benzerga AA. Modeling damage accumulation to fracture in a magnesium-rare earth alloy. Acta Mater 2017;124:225–36.
[54] Wasik A, Leszczynska-Madej B, Madej M, Rubach R, Garbiec D. Effect of holding time on densification, microstructure and selected properties of spark plasma sintered AA7075-B_4C composites. Materials 2022;15.
[55] Gallardo-Lopez A, Dominguez-Rodriguez A, Estournes C, Marder R, Chaim R. Plastic deformation of dense nanocrystalline yttrium oxide at elevated temperatures. J Eur Ceram Soc 2012;32:3115–21.
[56] Alizadeh A, Maleki M, Abdollahi A. Preparation of super-high strength nanostructured B_4C reinforced Al-2Cu aluminum alloy matrix composites by mechanical milling and hot press method: microstructural, mechanical and tribological characterization. Adv Powder Technol 2017;28:3274–87.
[57] Alizadeh A, Abdollahi A, Biukani H. Creep behavior and wear resistance of Al 5083 based hybrid composites reinforced with carbon nanotubes (CNTs) and boron carbide (B_4C). J Alloy Compd 2015;650:783–93.